



This is a repository copy of *Retention mechanism of cesium in chabazite embedded into metakaolin-based alkali activated materials*.

White Rose Research Online URL for this paper:

<https://eprints.whiterose.ac.uk/190403/>

Version: Published Version

Article:

Chaerun, R.I., Soonthornwiphat, N., Toda, K. et al. (7 more authors) (2022) Retention mechanism of cesium in chabazite embedded into metakaolin-based alkali activated materials. *Journal of Hazardous Materials*, 440. 129732. ISSN 0304-3894

<https://doi.org/10.1016/j.jhazmat.2022.129732>

Reuse

This article is distributed under the terms of the Creative Commons Attribution (CC BY) licence. This licence allows you to distribute, remix, tweak, and build upon the work, even commercially, as long as you credit the authors for the original work. More information and the full terms of the licence here:

<https://creativecommons.org/licenses/>

Takedown

If you consider content in White Rose Research Online to be in breach of UK law, please notify us by emailing eprints@whiterose.ac.uk including the URL of the record and the reason for the withdrawal request.



eprints@whiterose.ac.uk
<https://eprints.whiterose.ac.uk/>



Research Paper

Retention mechanism of cesium in chabazite embedded into metakaolin-based alkali activated materials



Raudhatul Islam Chaerun^{a,*}, Natatsawas Soonthornwiphat^a, Kanako Toda^c, Kazuma Kuroda^a, Xiaobo Niu^a, Ryosuke Kikuchi^b, Tsubasa Otake^b, Yogarajah Elakneswaran^b, John L. Provis^d, Tsutomu Sato^b

^a Division of Sustainable Resources of Engineering, Graduate School of Engineering, Hokkaido University, Sapporo 060-8628, Hokkaido, Japan

^b Division of Sustainable Resources of Engineering, Faculty of Engineering, Hokkaido University, Sapporo 060-8628, Hokkaido, Japan

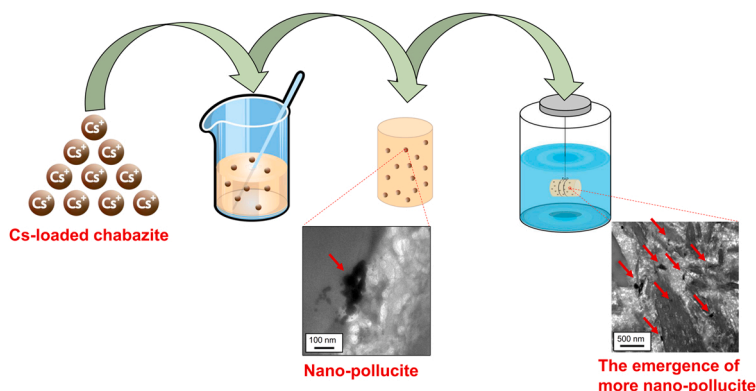
^c Nuclear Professional School, School of Engineering, The University of Tokyo, 2-22 Shirakata Shirane, Tokai-mura, Ibaraki 319-1188, Japan

^d Department of Materials Science and Engineering, The University of Sheffield, Sir Robert Hadfield Building, Mappin St, Sheffield S1 3JD, United Kingdom

HIGHLIGHTS

- K was responsible for the breakdown and reconstruction of the chabazite structure.
- Heterogeneous nano-pollucite was formed within the chabazite at 25 °C.
- The structure of chabazite was labile in the K-AAM environment.
- The chabazite ring was able to rebuild to form more pollucite.

GRAPHICAL ABSTRACT



ARTICLE INFO

Editor: Dr. T Meiping

Keywords:

K-based AAM
Pollucite
Chabazite
TEM
FE-EPMA, Raman spectroscopy

ABSTRACT

Disposal of cesium-137 (Cs-137)-loaded chabazite generated from decontaminating cooling water of the damaged reactor at the Fukushima Daiichi Nuclear Power Station (FDNPS) has become a crucial concern. The potassium aluminosilicate-based alkali activated material (K-AAM) matrix is one of the candidate encapsulation matrices proposed for encapsulating cesium-137. In this study, chabazite loaded with a low Cs concentration (1 mg/g of Cs), embedded into a K-AAM matrix (K-AAM-C), was analysed to determine its capability to immobilise Cs, which was investigated by batch leaching experiments, field emission-electron probe microscopy analysis (FE-EPMA), X-ray diffraction (XRD), transmission electron microscopy (TEM), and Raman spectroscopy. The leaching experiments revealed that K-AAM-C efficiently immobilised Cs, with only 3 % of the Cs leached out after 360 days of leaching in deionised water. Characterisation using XRD, TEM, and Raman analysis confirmed that the alkali-activator was responsible for the phase transformation of chabazite. FE-EPMA demonstrated that K entered the chabazite structure. This phenomenon resulted in the breakdown and subsequent reconstruction of

* Corresponding author.

E-mail addresses: chaerunislam96@gmail.com, Raudhatulislam.chaerun.v0@elms.hokudai.ac.jp (R.I. Chaerun).

<https://doi.org/10.1016/j.jhazmat.2022.129732>

Received 13 April 2022; Received in revised form 4 July 2022; Accepted 6 August 2022

Available online 8 August 2022

0304-3894/© 2022 The Authors. Published by Elsevier B.V. This is an open access article under the CC BY license (<http://creativecommons.org/licenses/by/4.0/>).

the chabazite structure. TEM observation showed that the Cs was concentrated into the aggregates of precipitates, heterogeneously forming a pollucite-like structure in the chabazite after the fabrication process. Thermodynamic calculations indicated that pollucite was preferably stable in an AAM environment. When immersed in water, the amount of nano-pollucite increased over time, leading to the structural re-arrangement of aluminosilicate rings of chabazite according to TEM and Raman analysis. Pollucite is well known as a Cs-bearing natural zeolite, which can encapsulate Cs in its structure. Therefore, Cs retention was achieved in the spent chabazite adsorbent embedded into the K-AAM due to the resultant pollucite structure formed during AAM fabrication.

1. Introduction

In March 2011, the earthquake and the consequent tsunami caused significant damage to Fukushima Daiichi Nuclear Power Station (FDNPS) in Japan. A huge volume of water has been injected to cool fuel debris in the damaged reactors. However, the coolant water has been contaminated with a large number of radionuclides such as cesium-137 (Cs-137) and strontium-90 (Sr-90). Especially, Cs-137 is a critical concern due to its high radioactivity and relatively long half-life (about 30 years). The contaminated coolant water was preliminarily treated to remove radioactive Cs and Sr using columns filled with adsorbents, and then subsequently treated by the Advanced Liquid Processing System (ALPS) to remove radionuclides except for tritium. These treatment processes have been producing radioactive wastes such as spent adsorbents and slurries since they began operation (TEPCO: *Contaminated Water Treatment*, n.d.). Therefore, the selection and development of optimised technologies for safe storage and disposal of the arising wastes are urgent issues at FDNPS.

Synthetic chabazite, a member of the zeolite group of aluminosilicate minerals, which has been used to remove radioactive Cs as an adsorbent in the KURION system and the Simplified Active Water Retrieve and Recovery System (SARRY) at FDNPS (Lehto et al., 2019). Due to the long-term treatment of contaminated water by these systems, a large volume of contaminated zeolite has been produced and stored in a temporary storage site at FDNPS, awaiting solidification before final long-term disposal (Harnett et al., 2019). The glass and ceramic materials that are sometimes used to solidify spent adsorbents exhibit excellent chemical and thermal stability. However, vitrification is relatively more expensive and may prove less practical for large-scale intermediate-level waste form manufacturing (Bernardo et al., 2012). A previous study indicates that the vitrification process may cause Cs to become volatile and evaporate, resulting in the production of secondary waste during the vitrification process (such as a high concentration of Cs radionuclide in the filter of melter off-gases) (Migge, 1989; Sargent, Jr, 1994; Yang et al., 2013).

On the other hand, cement-based materials have been widely adopted for solidification of spent adsorbents due to their low cost and ease of manufacture. However, conventional Portland cement is not favourable for radioactive Cs immobilization because the hydrate phases which form as it hardens are not capable of chemically immobilising Cs (El-Dessouky et al., 2013). Chemists and material scientists have discovered that alkali-activated materials (AAM) can be an excellent alternative to conventional cementitious materials, as they can immobilise hazardous wastes and be resistant to fire, acid, corrosion, and microbes, and have high compressive strength (Luukkonen et al., 2019; Mejía de Gutiérrez et al., 2020; Provis, 2018; Rasaki et al., 2019; Soonthornwiphat et al., 2020). In terms of chemistry, low-calcium AAMs have some similar chemical characteristics to zeolites, with a continuous cross-linked network of aluminate and silicate tetrahedral, charge-balanced by an alkali metal such as Na or K, but lacking long-range chemical ordering (Walkley et al., 2020). For this reason, the charge-balancing alkali cation is exchangeable due to its ionic bonding; this means that Cs can potentially replace Na as a balance cation in the aluminosilicate (Ichikawa et al., 2020; Niu et al., 2022), as long as the pore structure of the aluminosilicate matrix enables it to enter and

migrate to the relevant locations in the binder.

Generally, Na-based alkali-activated materials have excellent encapsulation properties for radionuclides such as Cs and Sr (Haddad et al., 2017; Walkley et al., 2020a). When Cs-loaded clinoptilolite is embedded within a Na-AAM, Cs⁺ can temporarily be an ionic bond with bonding oxygen of Al based on a soft Lewis acid-base mechanism (Kuenzel et al., 2015). It has been reported that K-AAM is substantially more effective than Na-AAM at immobilizing Cs and Sr, preserving amorphosity for high immobilisation, and exhibiting high flow properties for in-situ manufacturing (Niu et al., 2022; Soonthornwiphat et al., 2020). However, both K-AAM and Na-AAM appear to be effective encapsulants for Sr-loaded titanate ion exchangers (Ke et al., 2019). It has also been reported that Cs can be efficiently immobilised in zeolite A embedded into K-AAM to produce a ceramic phase (such as pollucite) with high-temperature (1100 °C) heat treatment (Li et al., 2022). However, there is, to date, no report on the Cs retention mechanism related to encapsulation of Cs-loaded chabazite particles in potassium-based AAM (K-AAM), particularly at very low Cs concentrations and at 25 °C. Therefore, in this study, the Cs retention mechanism in the chabazite embedded into the K-AAM matrix was investigated for the long-term safety of radionuclide disposal. It is required to clarify the radionuclide retention mechanism in the adsorbent embedded into the encapsulation matrix in order to better comprehend radionuclide decontamination for environmental management, since the behaviour of low-concentration Cs within chabazite embedded in K-AAM remains unknown. Therefore, the aims of this study are to determine possible Cs retention mechanisms and chabazite interactions in the K-AAM matrix.

2. Materials and methods

2.1. Materials and reagents

The precursor used to fabricate the AAMs was a commercial metakaolin (MetaStar 501, Imerys, UK), which had a high amorphous degree suitable for achieving a high degree of reaction and a desirable AAM structure. The metakaolin has a mean particle size of 3.90 µm and a chemical composition that is primarily composed of SiO₂ and Al₂O₃, as shown in Table 1. Alkali-activator solutions were prepared by using

Table 1
Chemical composition of starting chabazite and starting metakaolin based on energy-dispersive X-ray fluorescence (EDXRF).

Component	IE-90 Chabazite (wt%)	Metastar 501 Metakaolin (wt%)
SiO ₂	68.46	52.54
Al ₂ O ₃	18.66	44.80
TiO ₂	0.39	0.97
Fe ₂ O ₃	3.76	0.50
Na ₂ O	8.11	0.29
K ₂ O	0.57	0.20
CaO	0.83	0.03
MnO	0.03	Nd ^a
MgO	0.66	0.00
P ₂ O ₅	0.03	0.05
L.O.I ^b	15.22	0.49

^a Nd: Not detected

^b L.O.I is loss of ignition at 1100 °C for 12 h

potassium silicate solution (29.3 wt% SiO₂, 22.1 wt% K₂O, manufacturer FUJIFILM Wako Pure Chemical Corporation, Osaka, Japan), KOH pellets (purity >86%, manufacturer KANTO CHEMICAL CO., INC, Tokyo, Japan), and ultra-pure water. The cesium chloride (CsCl) was obtained from FUJIFILM Wako Pure Chemical Corporation, Osaka, Japan, for making the artificial Cs-loaded chabazite. The chabazite used was Ionsiv IE-90 (UNION SHOWA K.K., Japan), the synthetic Na-based chabazite with a particle size range of 48–590 μm and chemical composition determined by X-ray fluorescence (XRF: MagiX PRO, Spectris Co., Ltd) analysis utilising the fusion bead method, as indicated in Table 1.

2.2. Sample preparation

2.2.1. Cesium sorption in the chabazite

Non-radioactive CsCl solution at a concentration of 75.24 μM (10 mg/L) was prepared in 1 L of ultra-pure water to load onto the chabazite. The mass ratio of chabazite to solution volume containing Cs was 1:100 (g/mL). The chabazite suspension in the solution was shaken at 160 rpm for 24 h; 99.97% of the Cs was adsorbed into the chabazite structure during the shaking. Then, the pellets were separated from the solution by 0.2 μm pore filtration and dried at ambient temperature until they achieved constant weight.

2.2.2. Manufacturing the specimens

The alkali-activator (K₂SiO₃ solution) was prepared by dissolving the KOH pellets in potassium silicate solution and ultra-pure water, at ratios designed to acquire a solution with molar ratios K₂O/SiO₂ = 1.0 and H₂O/K₂O = 11. The AAM was then formulated to give a molar ratio of Al₂O₃ (from the metakaolin) to K₂O (from the alkali-activator) of 1.0. The final stoichiometry of the AAM was K₂O·Al₂O₃·3SiO₂·0.11 H₂O, and this ratio was proposed from our previous studies to obtain a stable AAM structure with good flowability for encapsulation (Ke et al., 2019; Soonthornwiphat et al., 2020). During the mixing process of alkali-activator and metakaolin to obtain AAM gel paste, Cs-loaded chabazite was added into the paste with a 0.30 mass ratio. The mixtures were manually blended for 15 min using a plastic rod and then cast into cylindrical PVC tube sections of 1.3 cm × 1.5 cm in size; both ends were sealed using Parafilm. The specimens were cured at 40°C for 24 h, then a further 24 h at 25°C.

The sample with encapsulated chabazite adsorbent is denoted K-AAM-C; samples without chabazite adsorbent were also prepared for comparative purposes, namely K-based AAM (K-AAM-WC), Na-based AAM (Na-AAM-WC) and ordinary Portland cement paste (OPC-WC). The recipe and preparation protocol of the AAM samples without chabazite adsorbent (K-AAM-WC and Na-AAM-WC) were identical to K-AAM-C samples, except that the Cs was added into AAM by different procedure; the CsCl was dissolved in the water before mixing with potassium silicate and KOH to obtain an activator containing 6.62 μM Cs, which was then mixed with metakaolin, stirred, poured into the mould, and sealed with Parafilm. For the cement paste samples, ordinary Portland cement (standard material '211 S' provided by Japan Cement Association) was mixed with water to give a liquid to solid ratio of 0.35. The CsCl was dissolved into the water before being mixed with cement paste to obtain 6.62 μM Cs. The fresh mixture was stirred, poured into the mould, and sealed with Parafilm, and cured at 25°C for 4 weeks.

2.3. Leaching experiments

The leaching experiments were conducted by immersing each specimen into 88 mL of deionised water based on the ANSI/ANS-16.1–2003 standard test. The ratio of the leachant volume to the specimen surface area was 10 mL/cm², and the leachant was replaced after cumulative leach times of 2 h, 7 h, and 1, 2, 3, 4, 5, 19, 47, 90, 150, 210, 270, 330, and 360 d from the onset of the experiments. The leachate was then analysed at each time point to determine the released Cs concentration

from the AAM matrix, and the solid specimens were removed after 90 and 360 days of the leaching experiment for solid-phase analysis.

2.4. Liquid-phase analysis

The solute after Cs sorption onto the chabazite adsorbent, and the leachates from the leaching experiments were analysed by inductively coupled plasma-mass spectroscopy (ICP-MS: iCAP Q ICP-MS, Thermo Scientific, USA) to determine the Cs leached fractions. The standard solution used was Costume Assurance Standard solution (10 mg/L Cs in 2 % HNO₃) of the SPEX CertiPrep from Metuchen, United States and was diluted to the range of 0.01–10 ppb using ultra-pure water. The pH values of the leachates were determined using a pH meter (model W-22XD, Horiba Ltd. Kyoto, Japan).

2.5. Solid-phase analysis

Samples of the starting chabazite, Cs-loaded chabazite, Cs-loaded chabazite embedded into AAM matrix, and Cs-loaded chabazite embedded into AAM matrix after being immersed into the deionised water, were analysed to determine any potential phase changes using X-ray diffraction (XRD: Rint2100, Rigaku, Japan), field emission-electron probe microanalyser (FE-EPMA: JXA-8530 F, JEOL, Japan), transmission electron microscopy (TEM: JEM-2010, JEOL, Japan), and Raman spectroscopy (micro-Raman spectroscopy by Via Reflex, Renishaw). Half of each sample was then crushed into a fine powder using an agate mortar and pestle, and loaded to a glass holder and then measured by XRD with a Cu-Kα radiation source at 30 kV and 20 mA, and a 2θ scan range from 2 to 70.

The other half portions of the samples were sliced, epoxied, and polished, then subjected to FE-EPMA analysis to obtain the elemental mapping of Cs, Na, K, Si, Al, and Fe in chabazite. For the targeted location in chabazite in the K-AAM-C sample, tungsten deposition was used to protect the targeted sample against gallium beam bombardment; then the targeted sample was sliced into a wedge shape with a size of 15 μm long, 2 μm wide, and ~8 μm high, ex-situ in a focused ion beam-secondary electron microscope (FIB-SEM: JEOL, JIB-4600 F). The sliced specimen was then lifted by an ex-situ micromanipulator and attached onto the tip of the OmniProbe lift-out TEM grid (EM Japan Co., Ltd, Japan), placed back into the FIB-SEM, and carefully trimmed to obtain a specimen size of less than 100 nm wide. The prepared samples were then observed by TEM with 80 keV acceleration voltage to prevent beam damage to fragile samples, and the reciprocal space measurement of diffuse rings was calculated using a DigitalMicrograph (GATAN).

The samples (starting chabazite, Cs-loaded chabazite, Cs-loaded chabazite embedded into the AAM matrix, and Cs-loaded chabazite embedded into the AAM matrix after being immersed into the deionised water) were also subjected to Raman spectroscopic analysis to determine any changes in the chabazite building-unit structure. The analysis conditions were 5% laser power adjusted at 0.15–30 mW, 532 nm excitation wavelength, scanning time of 10 s, and 5 scanned spectra averaged per analysis. The samples were epoxied and polished before being analysed by Raman spectroscopy, and the laser was directed on the selected target chabazite.

2.6. Thermodynamic calculation

The Geochemist's Workbench® (GWB ver.14, Bethke, 2008) software was used to determine the solubility diagram of the chabazite, which was derived from Thermochemical and Mineralogical Tables of Geochemical Modelling (Thermmodem v1.10 (<http://thermodem.brgm.fr>)) database and other sources of literature (Table 2) for possible transformation into K-, Na-, and Cs-zeolites. The ACT2 module in the software was used to determine the chabazite solubility diagrams in an aluminosilicate environment, and GSS was used to calculate the silica activity value by using an extended Debye-Hückel equation.

Table 2

The thermodynamic database for the possible change of K-, Na-, and Cs-zeolites.

Minerals name	Chemical composition	Sources
Phillipsite(Na)	NaAlSi ₃ O ₈ ·3 H ₂ O	thermoddem
Clinoptilolite (Na)	Na _{1.1} (Si _{4.9} Al _{1.1}) O ₁₂ ·2.7 H ₂ O	thermoddem
Heulandite(Na)	Na _{2.14} Al _{2.14} Si _{6.86} O ₁₈ ·6.17 H ₂ O	thermoddem
Chabazite(Na)	Na ₂ Al ₂ Si ₄ O ₁₂	thermoddem
Zeolite X	Na ₂ Al ₂ Si _{2.5} O ₁₂ ·6.2 H ₂ O	Lothenbach et al. (2019)
Zeolite Y	Na ₂ Al ₂ Si ₄ O ₁₂ ·8 H ₂ O	Lothenbach et al. (2019)
Analcime (Na)	Na _{0.99} Al _{0.99} Si _{2.01} O ₆ ·H ₂ O	thermoddem
Amorphous silica	SiO ₂	thermoddem
Pollucite	Cs _{0.84} Na _{0.11} (Al _{0.88} Si _{2.0})(O ₆)·0.17 H ₂ O	Ogorodova et al. (2003)
Phillipsite (K)	KAlSi ₃ O ₈ ·3 H ₂ O	thermoddem
Clinoptilolite (K)	K _{1.1} (Si _{4.9} Al _{1.1}) O ₁₂ ·2.7 H ₂ O	thermoddem
Heulandite (K)	K _{2.14} Al _{2.14} Si _{6.86} O ₁₈ ·6.17 H ₂ O	thermoddem
Chabazite (K)	K ₂ (Al ₂ Si ₄)O ₁₂ ·6 H ₂ O	thermoddem
Feldspar (K)	KAlSi ₃ O ₈	thermoddem

3. Results and discussion

3.1. Cs leaching behaviour in the cement and AAM matrix

The leaching of Cs from the samples tested is shown in Fig. 1a. Cs was leached out consistently from OPC-WC and Na-AAM-WC, which achieved leaching extents of 80 % and 16 % after 360 days, respectively. By comparison, K-AAM-WC and K-AAM-C showed Cs leaching extents of 11 % and 3 % after 360 days, respectively (Fig. 1b). Obviously, K-AAM-C was the best-performing matrix for Cs immobilisation, consistent with the presence of chabazite within the matrix. The Cs leaching behavior from each of the samples is explained in two stages: initial leaching (from 2 h to 18 days) and after 19 days of leaching (from 19 days to 360 days). This is due to the fact that the initial and later leaching trends of Cs have different Cs retention mechanisms from the perspective of the leaching curve.

As shown in Fig. 1a, during the initial leaching, the Cs bound with the Portland cement structure was extensively leached, representing the highest cumulative leaching fraction among the other matrices. This behaviour indicated that calcium silicate hydrate (C-S-H) in the cement does not have the necessary structure to support strong Cs immobilisation, consistent with the broader literature on this topic (Jiang et al., 2017; Viallis-Terrisse et al., 2001). However, a small amount of Cs within the cement could be slightly retarded on its surface due to weak adsorption on the layers of C-S-H (Jiang et al., 2017), although most Cs was leached out within the 360-day leaching test. Cs leaching from the Na-AAM-WC was initially higher than from the K-AAM-WC during the initial leaching period. This behaviour was presumably due to surface wash-off caused by the unbound Cs⁺ ions in the K-AAM-WC and

Na-AAM-WC pore solutions. However, the Na-AAM-WC nanostructure may have formed restrictive (e.g. cage-like) structure that could not physically contain the large Cs⁺ ions, while the K-AAM-WC structure was less ordered and thus offered the potential for unbound Cs⁺ to be physically confined, as Cs⁺ is more similar in ionic size to the charge-balancing K⁺ than Na⁺ (Huang et al., 2016; Marvila et al., 2021; Papa et al., 2018; Provis et al., 2015; Ramasamy et al., 2015). Therefore, the initial leaching of Cs from K-AAM-WC was much lower than from Na-AAM-WC. Eventually, after 19 days of leaching, the remaining Cs⁺ in both AAMs was gradually leached out, possibly via ion exchange processes and demonstrating that Cs was only moderately strongly bonded to Al-O sites in the aluminosilicate framework (Niu et al., 2022).

In the K-AAM-C, Cs was initially leached out to a leaching fraction of only 1 % after 19 days of leaching, and then remained relatively constant for another 341 days, yielding a final leaching fraction of 3% at the end of the experiment (360 days). The initial Cs leaching from the K-AAM-C is attributed to a small degree of Cs⁺ liberation from the chabazite surface due to surface attack by alkali-activator during the fabrication process, where this Cs⁺ would then be incorporated throughout the bulk of the AAM matrix and then follows similar mechanisms to those described above for the K-AAM-WC sample. Moreover, some of the chabazite grains will have been positioned at or very near the surface of the AAM, where the adsorbed Cs could be leached without any hindrance from the AAM matrix. Therefore, when the sample was immersed into the solution, some Cs⁺ was released during this initial leaching. After 19 days, Cs leaching from the K-AAM-C was significantly lower and more stable than in the K-AAM-WC. Additionally, after 19 days of leaching up to 360 days of leaching, Na-AAM-WC and K-AAM-WC showed modest Cs leaching compared to stable K-AAM-C. This behaviour is owing to the alkaline environment possessed by AAM, which may induce the structure to collapse and liberate Cs and K or Na, a process that requires time (Sindhunata et al., 2008). It has also been reported that Cs in Na-based alkali-activated materials forming zeolite F exhibits a similar leaching trend to that in Na-AAM-WC and K-AAM-WC, both of which gradually leach out, indicating that zeolite phases cannot maintain the best performance of Cs immobilisation compared to K-AAM-C, which is much more stable even after 360 days of leaching (Haddad et al., 2017). The stability of Cs within K-AAM-C is not yet fully understood, in particular the interactions between the AAM and the chabazite, and so it is important to further analyse the stability of Cs in the K-AAM-C matrix.

3.2. Elemental distribution in the K-AAM-C samples before and after leaching

The FE-EPMA analysis of the chabazite and AAM matrix in the cross-section sample (shown in Fig. 2) was carried out at 0 (before leaching), 90, and 360 days (after leaching). FE-EPMA detected a low concentration of Cs, which remained within the chabazite and AAM matrix before

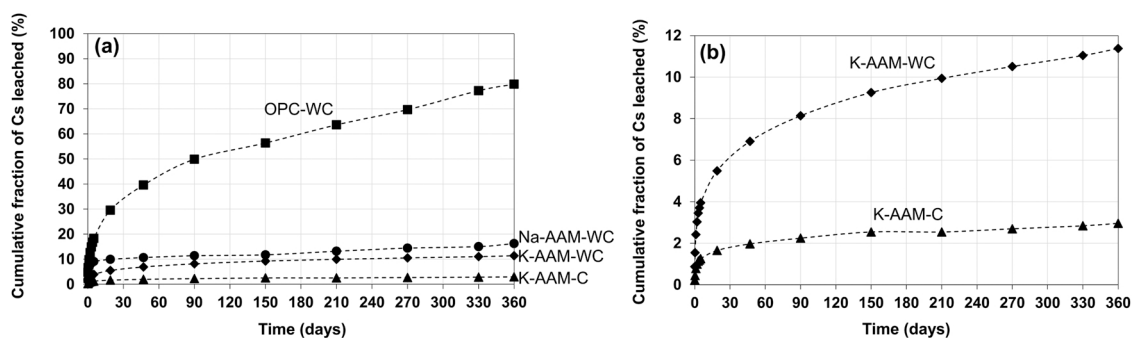


Fig. 1. (a) Cumulative fraction of cesium (Cs) leaching from OPC-WC (ordinary Portland cement without chabazite adsorbent), Na-AAM-WC (Na-based alkali-activated materials without chabazite adsorbent), K-AAM-WC (K-based alkali-activated materials without chabazite adsorbent), and K-AAM-C (K-based alkali-activated materials with chabazite adsorbent) for 360 days of leaching; (b) The enlarged curve of cumulative cesium (Cs) leaching from K-AAM-WC and K-AAM-C.

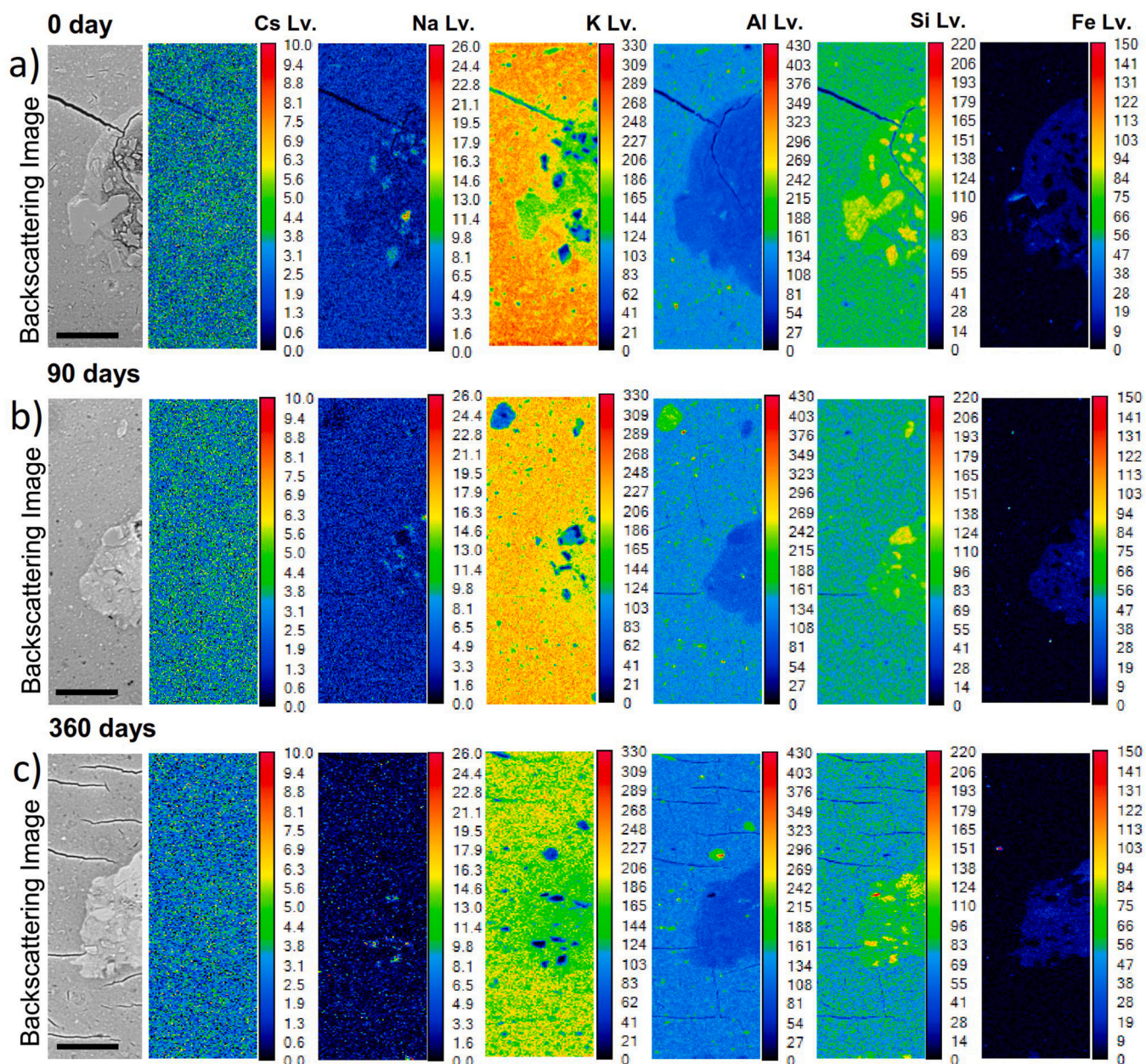


Fig. 2. Field emission - electron probe microscopy analysis (FE-EPMA) elemental mapping images of the K-AAM-C (K-based alkali-activated materials with chabazite adsorbent) at 0 days of leaching (a), 90 days of leaching (b), and 360 days of leaching (c). The scale bar of the backscattering images is 50 μm , and the value of Lv (level) on the scale bar is proportional to the count.

and after leaching. A small amount of Cs might have been released from chabazite during the AAM fabrication process due to a surface attack on the chabazite by the alkali-activator. Therefore, just after mixing (0 day), Cs was distributed within both the AAM matrix and chabazite adsorbent (Fig. 2a). Cs also remained in the chabazite adsorbent after 90 days (Fig. 2b) and 360 days (Fig. 2c) of leaching but experienced slow leaching from the AAM matrix, as indicated by a decrease in Cs intensity in areas corresponding to the AAM matrices. Si and K were dissolved from the chabazite adsorbent and AAM matrix, while an insignificant change of Al distribution was observed after 90 days of leaching. At the onset of the experiment (0 day), free K was quickly incorporated into chabazite and occupied any vacant or protonated charge-balancing sites at aluminates due to higher permeability with transient association with water from the alkali-activator. As a result, the K in chabazite was not well distributed throughout the chabazite due to an incomplete incorporation process, and so was less distributed than in the AAM matrix as a

result. Hence, there is a clear boundary surrounding the chabazite as shown in the backscattered image (BSE image) in Fig. 2a. After the K-AAM-C was immersed into deionised water, the free K was partially weakly bonded to the inner surfaces of the pores, and could easily be leached out in the presence of water. Moreover, the free K had migrated continuously into chabazite, leading to the disappearance of the elemental concentration boundary, which indicated that K had become equally distributed within the chabazite and AAM matrix (Figs. 2b-2c) through an ion exchange process.

On the other hand, Na remained heterogeneously within the chabazite after 90 days of leaching and was almost completely released after 360 days, and some remained within the AAM matrix (Figs. 2a-2c). The phenomenon of Na release might correspond to higher selectivity of K within the aluminosilicate than Na (Duxson et al., 2006); thus, Na had released from chabazite due to soft acids and bases selectivity in which Al in bonding oxygen (soft base) with low negative charge density

prefers K compared to Na (soft acids) with the lowest charge density (Kuenzel et al., 2015; Shannon, 1976; Sreenivasan et al., 2021). This soft acid and bases theory of cation selectivity in the bonding oxygen of Al in chabazite can also be applied to the bonding oxygen of Al in the AAM, which is analogous. Consequently, Na was gradually released from the AAM.

The small amount of Fe present remained within the chabazite even after 360 days of leaching. Impurity element Fe could replace Al isomorphically in the aluminosilicate structure without affecting the interaction (Ke et al., 2022). The cracks in the AAM matrix were due to water evaporation during drying before the thin section preparation. Therefore, a metakaolin-based AAM tended to shrink and crack when the water was removed from its pore structure (Kuenzel et al., 2015).

3.3. Evolution of the constituent materials during manufacturing and leaching and Cs retention mechanism

The chabazite used in this study possessed quartz and chabazite crystals (Fig. 3a), whereas the metakaolin possessed minor quartz, mica, anatase, kaolinite, and mainly the amorphous phase of the metakaolin structure characterised by a broad peak at $2\theta = 20^\circ$ (Fig. 3b). Most of the peaks disappeared from an AAM matrix containing Cs-loaded chabazite, except for quartz (Fig. 4a). The broad hump of metakaolin was shifted into an AAM hump of around $2\theta = 20\text{--}40^\circ$. The loss of intensity from the peaks representing the chabazite structure was presumably due to the partial disordering of the aluminosilicate rings and cages of the chabazite framework caused by the K-alkali activator and dominance of amorphous AAM structure to form an amorphous phase. This brought about a challenge to characterize the mineral phases of the samples of 90 days leaching (Fig. 4b) and 360 days leaching (Fig. 4c). However, the

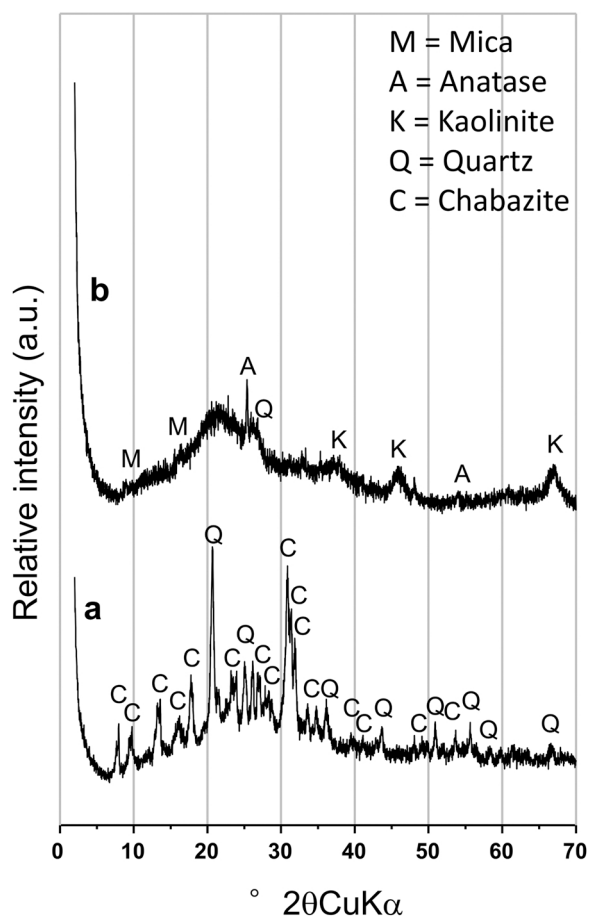


Fig. 3. X-ray diffraction pattern of starting chabazite (a) and metakaolin (b).

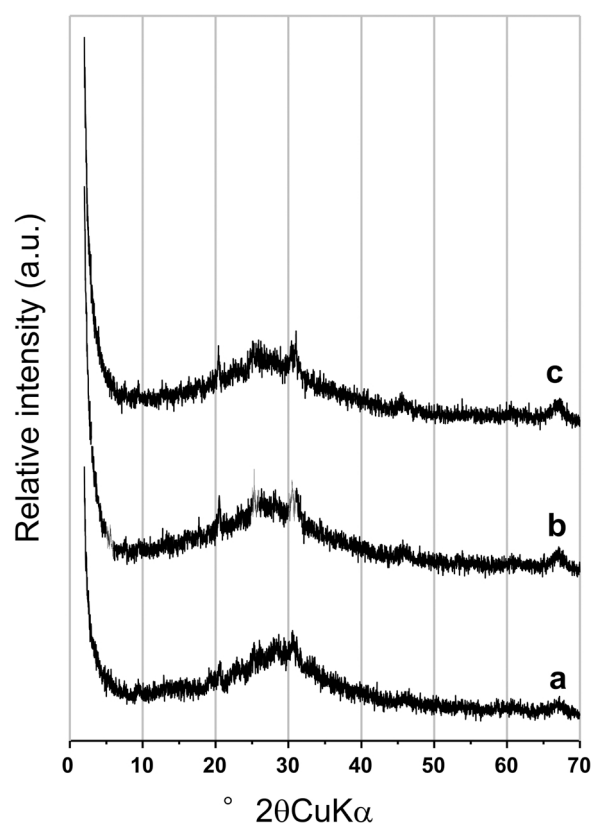


Fig. 4. X-ray diffraction patterns of K-AAM-C (K-based alkali-activated materials with chabazite adsorbent) at 0 days of leaching (a), 90 days of leaching (b), and 360 days of leaching (c).

BSE image of FE-EPMA showed that the bulk of the chabazite remained, and the boundary between the chabazite and AAM matrix was also discernible (Fig. 2). The presence of the dominant amorphous phase after chabazite was embedded into the K-AAM matrix showed that the K-AAM matrix environment resulted in a change in the chabazite crystal structure. However, the XRD analysis was not conclusive regarding the secondary phase of chabazite with this disordered or amorphous phase condition.

The FIB lift-out specimens of the K-AAM-C before and after 90 days of leaching were observed by TEM to obtain a more detailed clarification (herein the images, electron diffraction pattern, and EDS), as shown in Fig. 5. The observation was quickly conducted before the destruction of the samples due to the strong irradiation of the electron beam. In a chabazite-containing AAM sample taken before the leaching experiment, nano-cluster particles were found by TEM within the chabazite (Fig. 5a (left)). As indicated by the red arrows, these are pollucite-cluster particles that have formed within the chabazite pores, which was characterised by electron diffraction to have a similar spacing of diffuse rings to the d -spacings of a pollucite crystal, as shown in Fig. 5a (middle) (Newnham, 1967): the brightest contrast of ~ 0.338 nm and a lower intensity at ~ 0.289 , which are similar to two of the strong reflections (400 and 332 peaks respectively) of pollucite. It was difficult to obtain clear diffuse rings due to low crystallinity. It is worth noting that pollucite has a channel system of ~ 0.28 nm (Yokomori et al., 2014), in which the new phase depicts a ring with a similar interplanar spacing and a newly formed channel system. The pollucite clusters had a size of around 5–200 nm. When the K-alkali activator is introduced, the Na bonded in chabazite is replaced, and the material becomes more amorphous due to the instability of the chabazite structure, which is consistent with the FE-EPMA and XRD data. Because of the amorphous nature of the structure, it can easily reassemble with the host ions, which have a low charge density.

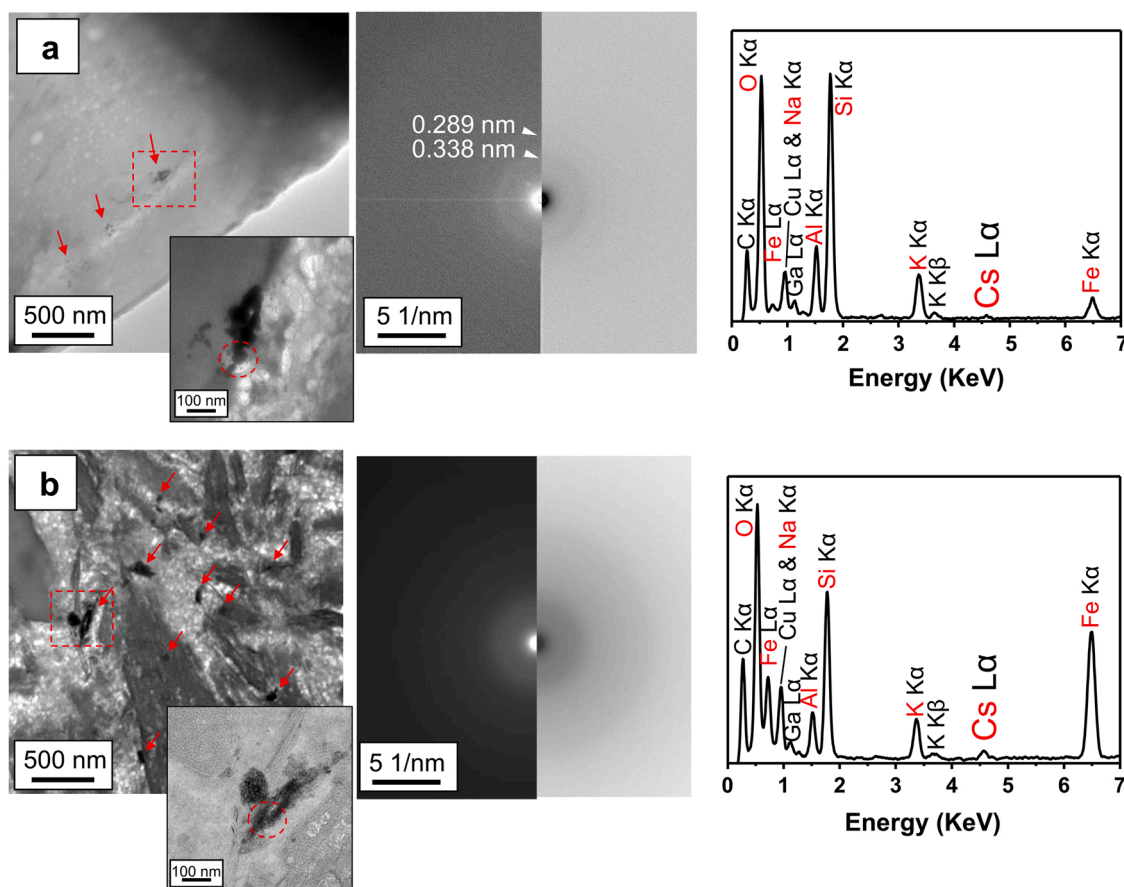


Fig. 5. Transmission electron microscopy (TEM) images, electron diffraction patterns, and energy-dispersive X-ray spectroscopy (EDS) spectra of the K-AAM-C (K-based alkali-activated materials with chabazite adsorbent) at 0 days of leaching (a) and 90 days of leaching (b). The formation of nano-pollucite can be seen in the TEM images by the red arrow marks.

Pollucite is most likely formed when K-chabazite recrystallises with Cs. This phenomenon will not occur when Na-chabazite is embedded into Na-AAM. The reason for this is that Na-AAM activator has a tendency to change Na-chabazite into other zeolites such as analcime, whereas Na-AAM transforms into zeolites such as zeolite X and zeolite A at 25 °C (Chiperu and Apps, 2001; Marvila et al., 2021). EDS was also used to analyse the nano-pollucite, showing a slight Cs L α peak associated with the impurity element Fe in aluminosilicate. New pollucite formation can occur under low temperatures in the chabazite. However, there is no previous literature available on the occurrence or formation of pollucite within chabazite embedded into K-AAM at 25 °C.

In a sample leached for 90 days, the chabazite crystals in the K-AAM were weakly diffracting and appeared brighter in the TEM image than in the unleached (0 day) sample. Most importantly, the population of the pollucite had increased, as shown by red arrows in Fig. 5b (left). Pollucite was unstable and became amorphous due to water loss by electron beam irradiation (Montagna et al., 2011). Therefore, the pollucite SAED pattern confirmed its amorphous structure (Fig. 5b (middle)).

The bulk analysis by Raman spectroscopy revealed the change of aluminosilicate tetrahedral structure in chabazite (Fig. 6), consisting of 4-, constructed a double 6-, 8-member rings (Knops-Gerrits et al., 1997). The most sensitive bands of chabazite rings in Raman spectroscopy were between 350 and 750 cm^{-1} , attributed to the vibration of the Si-O-Si, Si-O-Al, and Al-O-Si bonds and giving information about ring vibrations. Bands at 375–432 cm^{-1} and 432–527 cm^{-1} represented 8-member rings (8 R) and double 6-member ring (D6R), respectively, while those at 527–727 cm^{-1} corresponded to the 4-member ring (4 R) of chabazite (Fig. 6). The strongest frequency represented 4 R (616 cm^{-1}), and thus the weakest frequencies indicated D6R (481 cm^{-1}) and 8 R (386 cm^{-1}).

The reason for this occurrence was that a 4 R bond initially constructed the chabazite structure to form D6R and 8 R. Thus, the formation of the 4 R bond was more intense than other larger rings (Dutta et al., 1988). The sodium ion was usually positioned in larger rings within chabazite, such as D6R and 8 R (Alberti et al., 1982). When Cs entered the chabazite rings during adsorption, the Cs ion was introduced into the larger vacant rings such as D6R and 8 R as a result of its greater ionic size. Thus, D6R and 8 R showed high stretching frequencies and shifted to 486 cm^{-1} (D6R) and 407 cm^{-1} (8 R), as shown in Fig. 6a, and made the 4 R structures somewhat crumpled (lower frequency and shifted to 627 cm^{-1}) due to larger ion occupation in the larger rings (Fig. 6b) (Kwon et al., 2021). In the 0 day sample, D6R and 8 R exhibited broad bands (Fig. 6c). However, the 4 R peak remained only slightly shifted, to 627 cm^{-1} .

These broad bands indicated a significant deformation or collapse of the Si-O-Si, Si-O-Al, and Al-O-Si bonding structures comprising D6R, and slightly also 8 R, which in turn affected the regularity of 4 R geometries. The deformation of rings was probably caused by strong alkali attack from the alkali-activator leading to ion exchange, and thus an electronic effect due to the high amount of K occupying aluminosilicate rings (Ridha et al., 2009). According to TEM data, pollucite had already formed in the 0 day sample. Therefore, these broad bands were probably due to the effect of pollucite formation. Due to their comparable ionic radii, Cs and K have a similarly low charge density, balancing the ruptured bridging oxygen of alumina during the chabazite reconstruction process (Shannon, 1976; Sreenivasan et al., 2021). Although a K-alkali-activator was responsible for pollucite formation, curing at 40 °C may accelerate the crystallisation process since pollucite could easily form at higher temperatures (although particularly above 200 °C

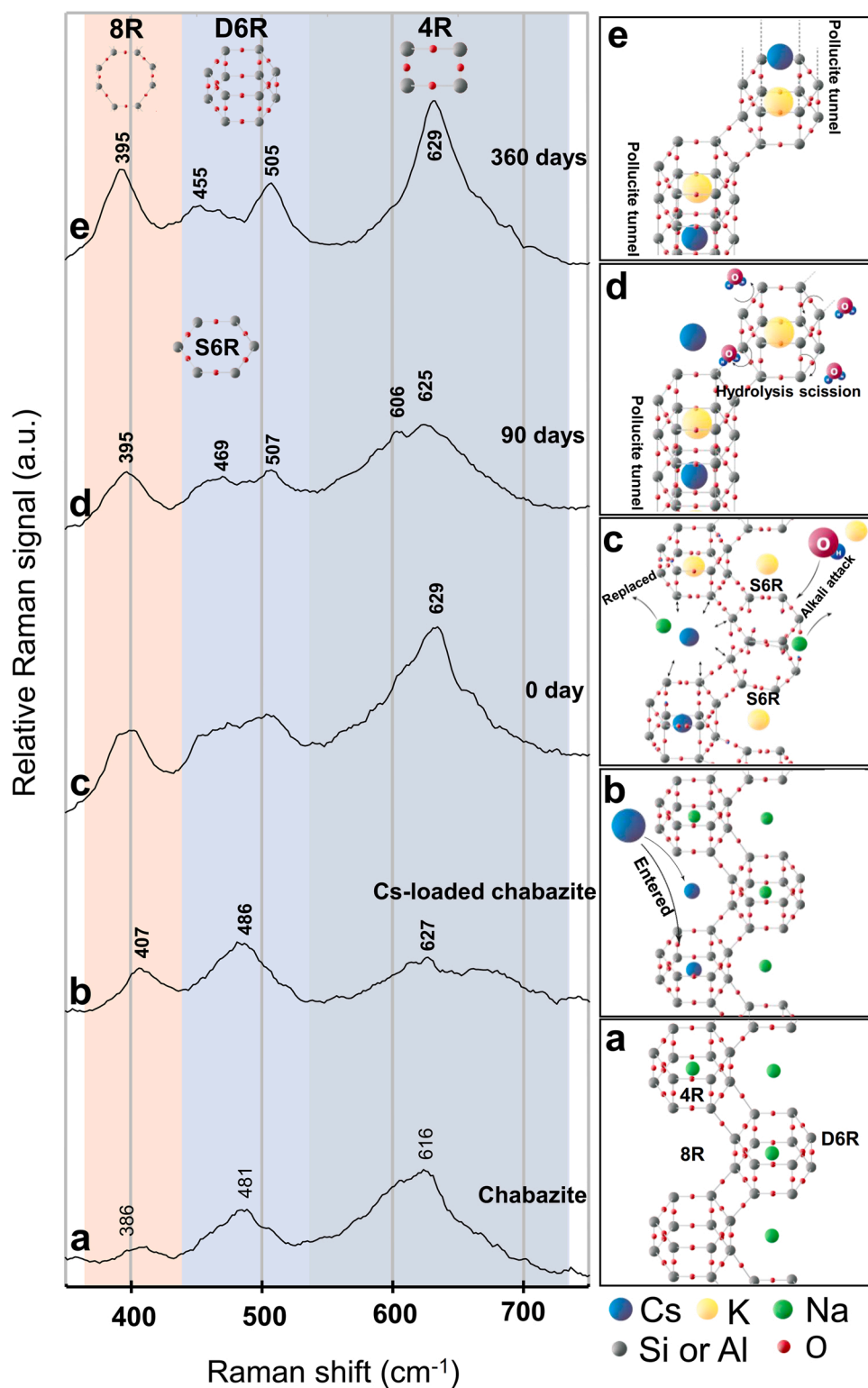


Fig. 6. Raman analysis of starting chabazite adsorbent (a), Cs-loaded chabazite adsorbent (b), and K-AAM-C (K-based alkali-activated materials with chabazite adsorbent) at 0 days of leaching (c), 90 days of leaching (d), and 360 days of leaching (e). Raman shifts represented the vibration of chabazite aluminosilicate rings, consisting of the 4-member ring (4 R) (375–432 cm^{-1}) in the dark grey background, double 6-member rings (D6R) (432–527 cm^{-1}) in the light bluish background, and 8-member ring (8 R) (527–727 cm^{-1}) in orange background.

(Dewaele et al., 1985)). The secondary phase evolution of chabazite to become pollucite was entirely possible, which agrees with TEM data. The structural reformation appeared after being immersed into water for 90 days, resulting in the ring-opening of D6R (507 cm^{-1}) into a single 6-member ring (S6R: 469 cm^{-1}) and D6R (507 cm^{-1}) as well as slightly decreasing and shifting the 4 R peak (625 cm^{-1}), and the emergence of a new peak (606 cm^{-1}) which represented asymmetric bending in 4 R (Fig. 6d).

This phenomenon might suggest that D6R structures were broken into S6R, which consequently affected 4 R formation. However, some D6R remained in the structure as a result of some structural reconnections to the original structure with substitution of K. Pollucite consisted of 4 R units building an overall aluminosilicate structure comprising S6R and 8 R, leading to the evolution of chabazite to form the pollucite structure (Shvanskaya et al., 2018). Furthermore, the peaks of 4 R and 8 R in the 360 days leaching specimen were positioned at the same shift

629 cm^{-1} (4 R) and 395 cm^{-1} (8 R) at which the ring was stable, whereas the construction of the S6R (455 cm^{-1}) and reconstruction of the D6R (505 cm^{-1}) structures for the 360 days leaching samples continued, probably caused by the framework scission effect by hydrolysis in the D6R units (Heard et al., 2019). This behaviour indicated that there was still spontaneous re-arrangement due to the lability of the K-chabazite structure via the D6R units, which associated with Cs to form pollucite, resulting in pollucite crystallisation within the chabazite. Thus, pollucite formation still occurred continuously, and in agreement with the TEM images, showing more pollucite formation and Cs retention by these pollucites after 90 days of leaching.

The stability diagram calculated by using the Act2 module in GWB (Fig. 7) shows that chabazite is stable under neutral and lower silica activity conditions in the Cs-K-Na-Si-Al-H₂O system. In the medium of pH 11.5 and higher activity of Si ($\log a_{\text{H}_4\text{SiO}_4}$ of -2.813), approaching the conditions used in the fabrication of K-AAM, pollucite is stable in the system for a long period of time and thus may be considered suitable for the final disposal of Cs-bearing wastes. Therefore, pollucite formation from chabazite, as mentioned above, is also thermodynamically supported in the presence of the alkali-activator.

4. Conclusions

The findings of the current work showed that spent chabazite adsorbents encapsulated by K-based AAMs immobilised Cs more effectively than when either Na-based AAM or OPC were used as encapsulants, based on the cumulative leached fraction of Cs over 360 days in deionised water. The crystallographically disordered nature of K-AAM, and its alkalinity, were the factors controlling K ion migration and the structural change of aluminosilicate rings in chabazite, thus leading to the formation of K-type chabazite and having similar amorphous properties to K-AAM. Cs and K had similar ionic radius and retention selectivity, which could confine both the Cs and K during the reconstruction of the aluminosilicate and yield crystallisation into pollucite during the AAM fabrication process. Na-AAM is well-known for relatively rapid crystallisation into zeolite at 25 °C; hence Na-AAM cannot induce the pollucite formation in the same way as K-AAM. The formation of pollucite continuously occurred during the leaching, in which the new structure of chabazite remained prone to the slow conversion to stable pollucite, as evidenced by Raman spectroscopy and TEM. Pollucite could be heterogeneously formed within the chabazite at low Cs concentrations and a temperature of 25 °C, which was different from many previous reports that exhibited ceramic pollucite formation at high temperatures. Thermodynamic modelling demonstrates that pollucite is stable in neutral and alkaline conditions, implying that pollucite will form continuously within chabazite and remain stable for an extended period of time. K-based AAM could be the best candidate for future cesium retention, thus providing a convincing option for long-term safe disposal.

Environmental implications

The Cs immobilisation mechanism in chabazite embedded in a potassium-based alkali-activated material matrix was investigated in this study. The findings of this study are novel since there is no report on the Cs immobilisation mechanism in the chabazite embedded into potassium-based alkali-activated materials to date. We believe that our study represents a significant contribution to the literature since it gives vital results on the encapsulation of radionuclides in alkali-activated materials, which are currently lacking in the field, and has a broad and significant impact on the environment, with a particular emphasis on radionuclide spent waste pollutants.

CRedit authorship contribution statement

Raudhatul Islam Chaerun: Conceptualization, Methodology,

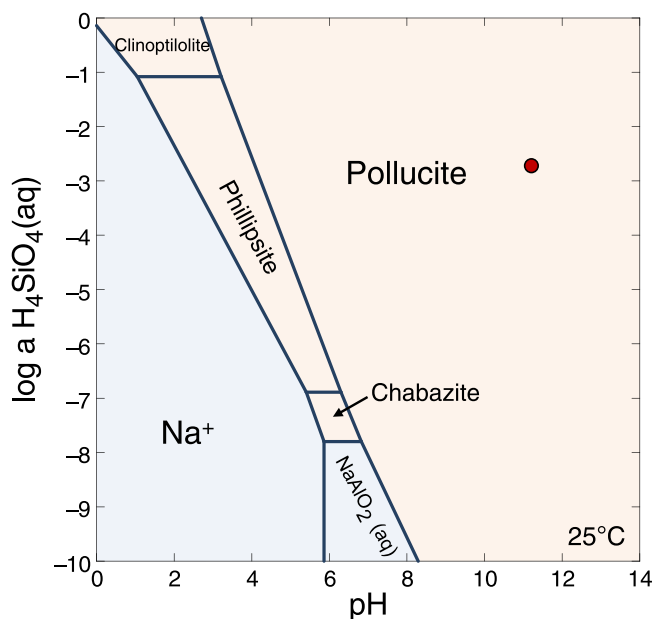


Fig. 7. The phase diagram of chabazite in potassium (K)-alkali activator environment. The yellow round mark indicated the changes of chabazite into pollucite at the high pH of 11.5 and $\log a_{\text{H}_4\text{SiO}_4}$ of -2.813 during the initial mixing at 25 °C.

Formal analysis, Software, Writing – original draft, Investigation, Data curation, Writing – review & editing. **Natatsawas Soonthornwiphat:** Investigation, Data curation, Writing – review & editing. **Kanako Toda:** Writing – review & editing. **Kazuma Kuroda:** Writing – review & editing. **Xiaobo Niu:** Writing – review & editing. **Ryosuke Kikuchi:** Methodology, Writing – review & editing. **Tsubasa Otake:** Writing – review & editing. **Yogarajah Elakneswaran:** Writing – review & editing. **John L. Provis:** Conceptualization, Funding acquisition, Writing – review & editing, Project administration. **Tsutomu Sato:** Conceptualization, Methodology, Funding acquisition, Supervision, Writing – review & editing, Project administration.

Declaration of Competing Interest

All authors declare that they have no competing interests.

Data Availability

Data will be made available on request.

Acknowledgements

This work was supported by JAEA Nuclear Energy S&T and Human Resource Development Project through concentrating wisdom, Grant Number JPJA19F19211936, "Nanotechnology Platform Program" of the Ministry of Education, Culture, Sports, Science and Technology (MEXT), Japan, Grant Number JPMXP09AA21HK0034, and The Engineering and Physical Sciences Research Council (EPSRC), United Kingdom, Grant Number EP/T013524/1. CRI gratefully acknowledges the scholarship provided by the Hashiya Scholarship Foundation during his study (2019–2023) at Hokkaido University (Master and Doctoral Program) and the JASSO (2018–2019) for the Master program. CRI also gratefully thanks Prof. Dr Takeda Yoshihiko and Dr Yamada Hirohisha for supporting his research and staying at the National Institute of Material Science.

References

- Alberti, A., Galli, E., Vezzalini, G., Passaglia, E., Zanazzi, P.F., 1982. Position of cations and water molecules in hydrated chabazite. *Natural and Na-, Ca-, Sr- and K-exchanged chabazites*. *Zeolites* 2 (4), 303–309. [https://doi.org/10.1016/S0144-2449\(82\)80075-4](https://doi.org/10.1016/S0144-2449(82)80075-4).
- Bernardo, E., Scarinci, G., Colombo, P., 2012. Vitrification of Waste and Reuse of Waste-Derived Glass. *ESST* 11581–11613. In: https://link.springer.com/referenceworkentry/10.1007/978-1-4419-0851-3_96#:~:text=Vitrification%20is%20a%20process%20comprising,quickly%20enough%20to%20prevent%20crystallization.
- Chipera, S.J., Apps, J.A., 2001. Geochemical stability of natural zeolites. *Rev. Mineral. Geochem.* 45 (1), 117–161. <https://doi.org/10.2138/rmg.2001.45.3>.
- Dewaele, N., Bodart, P., Gabelica, Z., Nagy, J.B., 1985. Synthesis and characterization of faujasite-type zeolites II. The role of alkali chlorides. *Stud. Surf. Sci. Catal.* 24 (C), 119–128. [https://doi.org/10.1016/S0167-2991\(08\)65276-3](https://doi.org/10.1016/S0167-2991(08)65276-3).
- Dutta, P.K., Shieh, D.C., Puri, M., 1988. Correlation of framework Raman bands of zeolites with structure. *Zeolites* 8 (4), 306–309. [https://doi.org/10.1016/S0144-2449\(88\)80127-1](https://doi.org/10.1016/S0144-2449(88)80127-1).
- Duxson, P., Provis, J.L., Lukey, G.C., Van Deventer, J.S.J., Separovic, F., Gan, Z.H., 2006. ^{39}K NMR of free potassium in zeolites. *Ind. Eng. Chem. Res.* 45 (26), 9208–9210. <https://doi.org/10.1021/ie060838g>.
- El-Dessouky, M.I., Sami, N.M., Abd El-Rehim, S.S., El-Gammal, B.H., 2013. Leaching study in immobilization of cesium and strontium radionuclides in Fly ash-zeolite cement. *Arab J. Nucl. Sci. Appl.* 46 (3), 52–62.
- Haddad, M.A., Ofer-Rozovsky, E., Bar-Nes, G., Borojovich, E.J.C., Nikolski, A., Mogiliansky, D., Katz, A., 2017. Formation of zeolites in metakaolin-based geopolymers and their potential application for Cs immobilization. *J. Nucl. Mater.* 493, 168–179. <https://doi.org/10.1016/j.jnucmat.2017.05.046>.
- Harnett, L.C., Gardner, L.J., Sun, S.K., Mann, C., Hyatt, N.C., 2019. Reactive spark plasma sintering of Cs-exchanged chabazite: characterisation and durability assessment for Fukushima Daiichi NPP clean-up. *J. Nucl. Sci. Technol.* 56 (9–10), 891–901. <https://doi.org/10.1080/00223131.2019.1602484>.
- Heard, C.J., Grajciar, L., Rice, C.M., Pugh, S.M., Nachtigall, P., Ashbrook, S.E., Morris, R. E., 2019. Fast room temperature lability of aluminosilicate zeolites. *Nat. Commun.* 10 (1) <https://doi.org/10.1038/s41467-019-12752-y>.
- Huang, X., Huang, T., Li, S., Muhammad, F., Xu, G., Zhao, Z., Yu, L., Yan, Y., Li, D., Jiao, B., 2016. Immobilization of chromite ore processing residue with alkali-activated blast furnace slag-based geopolymer. *Ceram. Int.* 42 (8), 9538–9549. <https://doi.org/10.1016/j.ceramint.2016.03.033>.
- Ichikawa, T., Watanabe, S., Arai, H., Haga, K., Yamada, K. (2020). Metakaolin-based geopolymer for immobilizing concentrated Cs generated by volume reduction of ^{137}Cs -contaminated waste. *Journal of the Society for Remediation of Radioactive Contamination in the Environment*, 8(1), 3–16. <http://hdl.handle.net/2115/79155%0A>.
- Jiang, J., Wang, P., Hou, D., 2017. The mechanism of cesium ions immobilization in the nanometer channel of calcium silicate hydrate: a molecular dynamics study. *Phys. Chem. Chem. Phys.* 19 (41), 27974–27986. <https://doi.org/10.1039/c7cp05437h>.
- Ke, X., Bernal, S.A., Sato, T., Provis, J.L., 2019. Alkali aluminosilicate geopolymers as binders to encapsulate strontium-selective titanate ion-exchangers. *Dalton Trans.* 48 (32), 12116–12126. <https://doi.org/10.1039/c9dt02108f>.
- Ke, Y., Liang, S., Hou, H., Hu, Y., Li, X., Chen, Y., Li, X., Cao, L., Yuan, S., Xiao, K., Hu, J., Yang, J., 2022. A zero-waste strategy to synthesize geopolymer from iron-recovered Bayer red mud combined with fly ash: roles of Fe, Al and Si. *Constr. Build. Mater.* 322 (September 2021), 126176 <https://doi.org/10.1016/j.conbuildmat.2021.126176>.
- Knops-Gerrits, P.P., De Vos, D.E., Feijen, E.J.P., Jacobs, P.A., 1997. Raman spectroscopy on zeolites. *Microporous Mater.* 8 (1–2), 3–17. [https://doi.org/10.1016/S0927-6513\(96\)00088-0](https://doi.org/10.1016/S0927-6513(96)00088-0).
- Kuenzel, C., Cisneros, J.F., Neville, T.P., Vandeperre, L.J., Simons, S.J.R., Bensted, J., Cheeseman, C.R., 2015. Encapsulation of Cs/Sr contaminated clinoptilolite in geopolymers produced from metakaolin. *J. Nucl. Mater.* 466, 94–99. <https://doi.org/10.1016/j.jnucmat.2015.07.034>.
- Kwon, S., Kim, C., Han, E., Lee, H., Cho, H.S., Choi, M., 2021. Relationship between zeolite structure and capture capability for radioactive cesium and strontium. *J. Hazard. Mater.* 408 (August 2020), 124419 <https://doi.org/10.1016/j.jhazmat.2020.124419>.
- Lehto, J., Koivula, R., Leinonen, H., Tusa, E., Harjula, R., 2019. Removal of radionuclides from Fukushima Daiichi waste effluents. *Sep. Purif. Rev.* 48 (2), 122–142. <https://doi.org/10.1080/15422119.2018.1549567>.
- Li, L., Xu, Z., Li, H., Li, J., Hu, D., Xiang, Y., Han, L., Peng, X., 2022. Immobilization of strontium and cesium by aluminosilicate ceramics derived from metakaolin geopolymer-zeolite A composites via 1100 °C heating treatment. *Ceram. Int.* 48 (11), 15236–15242. <https://doi.org/10.1016/j.ceramint.2022.02.054>.
- Lothenbach, B., Kulik, D.A., Matschei, T., Balonis, M., Baquerizo, L., Dilnesa, B., Miron, G.D., Myers, R.J., 2019. *Cemdata18: A chemical thermodynamic database for hydrated Portland cements and alkali-activated materials*. *Cem Concr Res* 115, 472–506.
- Luukkonen, T., Heponiemi, A., Runtti, H., Pesonen, J., Yliniemi, J., Lassi, U., 2019. Application of alkali-activated materials for water and wastewater treatment: a review. *Rev. Environ. Sci. Biotechnol.* 18 (2), 271–297. <https://doi.org/10.1007/s11157-019-09494-0>.
- Marvila, M.T., Azevedo, A.R.G., Delaqua, G.C.G., Mendes, B.C., Pedroti, L.G., Vieira, C. M.F., 2021. Performance of geopolymer tiles in high temperature and saturation conditions. *Constr. Build. Mater.* 286, 122994 <https://doi.org/10.1016/j.conbuildmat.2021.122994>.
- Mejía de Gutiérrez, R., Villalquira-Caicedo, M., Ramírez-Benavides, S., Astudillo, M., Mejía, D., 2020. Evaluation of the antibacterial activity of a geopolymer mortar based on metakaolin supplemented with TiO₂ and CuO particles using glass waste as fine aggregate. *Coatings* 10 (2), 1–16. <https://doi.org/10.3390/coatings10020157>.
- Migge, H., 1989. Simultaneous evaporation of CS and TC during vitrification-A thermochemical approach. *MRS Online Proc. Libr.* 176 (1), 419. <https://doi.org/10.1557/PROC-176-411>.
- Montagna, G., Arletti, R., Vezzalini, G., Di Renzo, F., 2011. Borosilicate and aluminosilicate pollucite nanocrystals for the storage of radionuclides. *Powder Technol.* 208 (2), 491–495. <https://doi.org/10.1016/j.powtec.2010.08.048>.
- Newham, R.E., 1967. Crystal structure and optical properties of pollucite. *Am. Mineral.* 52 (9–10), 1515–1518.
- Niu, X., Elakneswaran, Y., Islam, C.R., Provis, J.L., Sato, T., 2022. Adsorption behaviour of simulant radionuclide cations and anions in metakaolin-based geopolymer. *J. Hazard. Mater.* 429 (January), 128373 <https://doi.org/10.1016/j.jhazmat.2022.128373>.
- Ogorodova, L.P., Melchakova, L.V., Kiseleva, I.A., Belitsky, I.A., 2003. Thermochemical study of natural pollucite. *Thermochim. Acta* 403 (2), 251–256.
- Papa, E., Medri, V., Amari, S., Manaud, J., Benito, P., Vaccari, A., Landi, E., 2018. Zeolite-geopolymer composite materials: production and characterization. *J. Clean. Prod.* 171, 76–84. <https://doi.org/10.1016/j.jclepro.2017.09.270>.
- Provis, J.L., 2018. Alkali-activated materials. *Cem. Concr. Res.* 114, 40–48. <https://doi.org/10.1016/j.cemconres.2017.02.009>.
- Provis, J.L., Palomo, A., Shi, C., 2015. Advances in understanding alkali-activated materials. *Cem. Concr. Res.* 78, 110–125. <https://doi.org/10.1016/j.cemconres.2015.04.013>.
- Ramasamy, S., Hussin, K., Abdullah, M.M.A.B., Ghazali, C.M.R., Sandu, A.V., Binhusain, M., Shahedan, N.F., 2015. Recent dissertations on kaolin based geopolymer materials. *Rev. Adv. Mater. Sci.* 42 (1), 83–91.
- Rasaki, S.A., Bingxue, Z., Guarecuco, R., Thomas, T., Minghui, Y., 2019. Geopolymer for use in heavy metals adsorption, and advanced oxidative processes: a critical review. *J. Clean. Prod.* 213, 42–58. <https://doi.org/10.1016/j.jclepro.2018.12.145>.
- Ridha, F.N., Yang, Y., Webley, P.A., 2009. Adsorption characteristics of a fully exchanged potassium chabazite zeolite prepared from decomposition of zeolite Y. *Microporous Mesoporous Mater.* 117 (1–2), 497–507. <https://doi.org/10.1016/j.micromeso.2008.07.034>.
- Sargent, Jr., T.N. (1994). Vitrification of cesium-contaminated organic ion exchange resin. <https://doi.org/10.2172/254955>.
- Shannon, R., 1976. Revised effective ionic radii and systematic studies of interatomic distances in halides and chalcogenides. *Acta Crystallogr.* A 32, 751–767. <https://doi.org/10.1023/A:1018927109487>.
- Shvanskaya, L.V., Yakubovich, O.V., Koshelev, A.V., Vasiliev, A.N., 2018. Metal-loaded pollucite-like aluminophosphates: dissymmetrisation of crystal structures and physical properties. *Phys. Chem. Miner.* 45 (7), 633–640. <https://doi.org/10.1007/s00269-018-0948-z>.
- Soonthornwiphat, N., Kobayashi, Y., Toda, K., Kuroda, K., Islam, C.R., Otake, T., Provis, J.L., Sato, T., 2020. Encapsulation of Sr-loaded titanate spent adsorbents in potassium aluminosilicate geopolymer. *J. Nucl. Sci. Technol.* 00 (00), 1–8. <https://doi.org/10.1080/00223131.2020.1775717>.
- Sreenivasan, H., Adesanya, E., Niu, H., Perumal, P., Kantola, A.M., Telkki, V.V., Huttala, M., Cao, W., Provis, J.L., Illikainen, M., Kinnunen, P., 2021. Evidence of formation of an amorphous magnesium silicate (AMS) phase during alkali activation of (Na-Mg) aluminosilicate glasses. *Cem. Concr. Res.* 145 (November 2020), 106464 <https://doi.org/10.1016/j.cemconres.2021.106464>.
- Viallis-Terrisse, H., Nonat, A., Petit, J.C., 2001. Zeta-potential study of calcium silicate hydrates interacting with alkaline cations. *J. Colloid Interface Sci.* 244 (1), 58–65. <https://doi.org/10.1006/jcis.2001.7897>.
- Walkley, B., Ke, X., Hussein, O.H., Bernal, S.A., Provis, J.L., 2020. Incorporation of strontium and calcium in geopolymer gels. *J. Hazard. Mater.* 382 (August 2019), 121015 <https://doi.org/10.1016/j.jhazmat.2019.121015>.
- Walkley, B., Page, S.J., Rees, G.J., Provis, J.L., Hanna, J.V., 2020. Nanostructure of CaO-(Na₂O)-Al₂O₃-SiO₂-H₂O gels revealed by multinuclear solid-state magic angle spinning and multiple quantum magic angle spinning nuclear magnetic resonance spectroscopy. *J. Phys. Chem. C* 124 (2), 1681–1694. <https://doi.org/10.1021/acs.jpcc.9b10133>.
- Yang, J.H., Shin, J.M., Lee, C.H., Heo, C.M., Jeon, M.K., Kang, K.H., 2013. Stabilization of Cs/Re trapping filters using magnesium phosphate ceramics. *J. Radioanal. Nucl. Chem.* 295 (1), 211–219. <https://doi.org/10.1007/s10967-012-1774-2>.
- Yokomori, Y., Asazuki, K., Kamiya, N., Yano, Y., Akamatsu, K., Toda, T., Aruga, A., Kaneo, Y., Matsuoka, S., Nishi, K., Matsumoto, S., 2014. Final storage of radioactive cesium by pollucite hydrothermal synthesis. *Sci. Rep.* 4, 14–17. <https://doi.org/10.1038/srep04195>.